Published in final edited form as:
J Mol Biol. 2012 August 10; 421(2-3): 378–389. doi:10.1016/j.jmb.2012.04.017.

Nucleobindin 1 Caps Human Islet Amyloid Polypeptide Protofibrils to Prevent Amyloid Fibril Formation

Ruchi Gupta[1], **Neeraj Kapoor**[1], **Daniel P. Raleigh**[2,*], and **Thomas P. Sakmar**[1,*]

[1]Laboratory of Biochemistry and Molecular Biology, The Rockefeller University, New York, NY 10065, USA

[2]Department of Chemistry, Graduate Program in Biochemistry and Structural Biology, and Graduate Program in Biophysics, State University of New York at Stony Brook, Stony Brook, NY 11794, USA

Abstract

Many human diseases are associated with amyloid fibril deposition, including type 2 diabetes mellitus (DM) where human Islet Amyloid Polypeptide (hIAPP) forms fibrils in the pancreas. We report here that engineered, soluble forms of the human Ca^{2+}-binding protein Nucleobindin 1 (NUCB1), prevent hIAPP fibril formation and disaggregate pre-existing hIAPP fibrils. Scanning transmission electron microscopy (STEM) and atomic force microscopy (AFM) indicate that NUCB1 binds to and stabilizes heterogeneous prefibrillar hIAPP species. The NUCB1-stabilized prefibrillar species were isolated by size-exclusion chromatography and analyzed by STEM, dynamic light scattering (DLS) and multi-angle light scattering (MALS). The stabilized prefibrillar species show a size-range of 2–6 million Da and have other similarities to hIAPP protofibrils, but they do not progress to become mature fibrils. The effects of NUCB1 are absent in the presence of Ca^{2+}. We postulate that the engineered forms of NUCB1 prevent hIAPP fibril formation by a mechanism where protofibril-like species are “capped” to prevent further fibril assembly and maturation. This mode of action appears to be different from other protein based inhibitors, suggesting that NUCB1 may offer a new approach to inhibiting amyloid formation and disaggregating amyloid fibrils.

Keywords

amylin; islet amyloid polypeptide; Type-2 diabetes mellitus; amyloid; Nucleobindin 1; NUCB1; protofibril; fibril

Introduction

Amyloid fibril deposition is a pathophysiological hallmark of a number of severe degenerative disorders, including Alzheimer’s disease, Creutzfeldt-Jacob disease, Parkinson’s disease and Huntington’s disease. Amyloid is also associated with type 2 diabetes mellitus (DM) and the systemic amyloidoses[1; 2; 3; 4; 5]. Amyloidogenic peptides and proteins, including unfolded, misfolded or partially denatured proteins, share no primary structural homology, but the general process of amyloid formation follows a characteristic

*To whom correspondence may be addressed.

SUPPORTING INFORMATION

Isothermal Calorimetric experiments showed no binding of *s*NUCB1 to a hIAPP mutant called Pramlintide, which is monomeric and shows no aggregation; data showing that the complex of *s*NUCB1 and hIAPP protofibrils is stable and does not degrade even after 7 days.

pathway[6; 7]. Peptides adopt beta-hairpin secondary structure and self-assemble into protofibrils with cross-beta sheet quaternary structure. The protofibrils pack to form filaments and mature fibrils. Amyloid fibrils, and especially their precursor protofibrillar species, appear to be toxic to cells and tissues[8; 9]. Proteins and peptides with amyloidogenic potential are present normally, and their unaggregated forms often play important roles in cell physiology and regulation. For example, human Islet Amyloid Polypeptide (hIAPP) is a natively unstructured pancreatic endocrine hormone that regulates food intake and fat storage[10]. It is co-secreted with insulin from pancreatic β-cells in response to glucose uptake[11]. hIAPP is a very hydrophobic peptide with a significantly high propensity to aggregate rapidly in aqueous solution *in vitro* even at low micromolar concentrations. Physiologically, the concentration of hIAPP in secretory granules can vary from 100 μM to 4 mM, but even at such high concentrations, hIAPP does not aggregate under the normal environment of secretory granules[12]. However, in type 2 DM, aggregation of hIAPP results in islet amyloid deposits, which are toxic to the insulin producing β-cells[11; 13].

Several peptide fragments and derivatives of hIAPP have been identified that inhibit fibril formation *in vitro* and a number of small molecule inhibitors have been reported, but new inhibitors are desired, especially since many existing ones work only in molar excess[14; 15; 16; 17; 18; 19; 20]. We investigated the ability of Nucleobindin 1 (NUCB1), a 55-kDa Ca^{2+}-binding protein that is widely expressed and is conserved from flies to humans, to inhibit hIAPP fibril formation[21]. We show that a form of NUCB1 engineered to be soluble, *s*NUCB1, inhibits hIAPP aggregation at sub-stoichiometric levels and effectively disaggregates preformed fibrils in the absence of Ca^{2+}. The anti-amyloidogenic activity of NUCB1 is lost in the presence of Ca^{2+}. Using scanning transmission electron microscopy (STEM) and atomic force microscopy (AFM) in conjunction with other biochemical methods, we demonstrate that Ca^{2+}-free *s*NUCB1 binds to and stabilizes a prefibrillar species of hIAPP. NUCB1 appears to “cap” a protofibril-like species, which inhibits its further assembly and growth. The *s*NUCB1-bound prefibrillar hIAPP species appears to be a “dead-end” complex that is incapable of seeding further aggregation of hIAPP.

RESULTS

A soluble form of NUCB1 inhibits amyoid fibril formation by hIAPP

NUCB1 is nominally considered to be a Golgi-resident Ca^{2+}-binding protein, but it is also found in the cytoplasm and nucleus, and can be secreted as well[22]. We first engineered a soluble form of NUCB1, called *s*NUCB1, for heterologous expression in *E. coli* as described earlier[23]. We then measured the aggregation kinetics of hIAPP alone and in the presence of different amounts of *s*NUCB1 using a conventional thioflavin-T (thio-T) fluorescence-binding assay (Fig. 1A). For hIAPP alone, aggregation starts with a nucleation phase of approximately 5 min under the conditions of our assay and extends into a growth/elongation phase between 5 and 20 min. The growth phase of the curve plateaus into a stationary phase where fibrils are in equilibrium with the soluble peptide. When *s*NUCB1 was incubated with hIAPP in the absence of Ca^{2+}, we observed a significant decrease in the overall enhancement of thio-T fluorescence and a change in the kinetics of fluorescence enhancement. The effect was maximal in the presence of an equimolar amount (32 μM) of *s*NUCB1 and hIAPP. The inhibition of the thio-T fluorescence increase was observed even at sub-stoichiometric ratios of *s*NUCB1 to hIAPP (Fig. 1A).

We used transmission electron microscopy (TEM) as a direct probe of amyloid fibril formation. hIAPP alone (32 μM) aggregates within 7 min to form oligomers, which continue to grow and form higher order intermediates, protofibrils and protofilaments, which can be observed as early as about 13 min. The protofibrillar intermediates assemble and extend into mature amyloid fibrils within 60 min (Fig. 1B). Reaction mixtures with stoichiometric or

lower concentrations of *s*NUCB1 were preincubated with hIAPP (32 μM) and analyzed using TEM (Fig. 1C). The samples withdrawn at 7 min and 13 min from reaction mixtures that contain 32 μM, 10.7 μM, 6.4 μM or 3.2 μM of *s*NUCB1, respectively, show oligomeric species, and the 60 min sample shows the presence of ordered prefibrillar species, which clearly differ from amyloid fibrils. Thus, *s*NUCB1 alters the normal amyloid assembly process and leads to the formation of prefibrillar aggregates that do not go on to form amyloid. The formation of prefibrillar species in each of these reactions explains the observed initial increase in the thio-T fluorescence shown in Figure 1. The absence of an apparent lag phase in the presence of *s*NUCB1 indicates that the protein might drive hIAPP to form prefibrillar species. However, conventional hIAPP fibrils were not observed in the presence of *s*NUCB1 in the TEM assay except at limiting concentrations of *s*NUCB1. In a control experiment, 32 μM Ca^{2+}-free *s*NUCB1 alone does not aggregate when incubated at room temperature (Fig. 1B)

NUCB1 is a dimeric multi-domain protein with two Ca^{2+}-binding EF hand domains. Ca^{2+} readily binds to *s*NUCB1 and induces conformational changes within the protein subunit[23]. We tested the effect of Ca^{2+}-bound *s*NUCB1 on hIAPP amyloid formation under conditions where Ca^{2+}-free *s*NUCB1 effectively inhibited fibril formation. Ca^{2+}-bound *s*NUCB1 had no significant effect on formation of hIAPP fibrils. TEM images of hIAPP incubated in the presence of *s*NUCB1 and Ca^{2+} (3 mM) show the presence of protofibrils and protofilaments at 15 min, which continue to grow into fibrillar structures. Mature hIAPP amyloid fibrils are seen in the 60 min sample (Fig 2). Fibrils were not observed under the identical conditions in the absence of Ca^{2+}.

Evidence that sNUCB1 disaggregates hIAPP fibrils

We investigated the ability of *s*NUCB1 to disaggregate preformed hIAPP fibrils. In the absence of Ca^{2+}, *s*NUCB1 effectively disaggregates hIAPP fibrils into smaller species within 15 min. These species do not re-associate to form fibrils even after 45 min of additional incubation (Fig. 3). As observed in the inhibition experiments, Ca^{2+} eliminated the ability of *s*NUCB1 to disaggregate hIAPP fibrils. TEM images corresponding to samples withdrawn after addition of equimolar amounts of *s*NUCB1 to fibrils in the presence of 3 mM Ca^{2+} show fibrillar species in the micrographs at all time points (Fig. 3).

The observation that *s*NUCB1 inhibits amyloid formation at substoichiometric concentrations suggests that it may bind to oligomeric hIAPP species, which implies that *s*NUCB1 should inhibit amyloid formation when added at the lag phase of the amyloid formation pathway. *s*NUCB1 was added at different points during the hIAPP aggregation process, in the lag phase (7 min), in the middle of growth phase (13 min) and in the steady-state plateau (40 min), and then incubated for an additional 60 min. TEM showed no amyloid fibrils in any of the samples. The 13 min time point showed prefibrillar species, which were different from the filaments observed in the absence of *s*NUCB1. As a control, TEM micrographs were recorded for each sample prior to the addition of *s*NUCB1 (Fig. 4). These results suggest that Ca^{2+}-free *s*NUCB1 possesses the ability to inhibit hIAPP amyloid fibril formation at any stage of the pathway.

*s*NUCB1 stabilizes hIAPP prefibrillar species

We characterized a mixture of *s*NUCB1 and hIAPP by size exclusion chromatography (SEC) (Fig. 5A). Since hIAPP contains only one Tyr and no Trp residues, *s*NUCB1 dominates the absorbance at 280 nm. The SEC chromatogram shows peaks at 7.6 ml (Peak 1) and 11.8 ml (Peak 2). Injection of a 32-μM solution of Ca^{2+}-free *s*NUCB1 alone onto the column generates a peak centered at 11.8 ml (Fig. 5A). The peaks were analyzed by dot blot analysis using an anti-NUCB1 antibody and an anti-IAPP antibody. The results of the dot

blot analysis show that *s*NUCB1 was present in both the Peak 1 and Peak 2 fractions, whereas hIAPP was present only in the Peak 1 fraction (Fig. 5B). Control experiments showed no cross reactivity for either antibody. Both fractions were further analyzed by TEM. The micrographs show the presence of only prefibrillar species in the Peak 1 fraction, whereas the Peak 2 fraction reveals an image similar to that observed for *s*NUCB1 in absence of hIAPP (Fig. 5C).

Multi-angle light scattering (MALS) and dynamic light scattering (DLS) analysis were performed to estimate the average molecular mass and hydrodynamic radii of the eluting species. MALS analysis of Peak 1 gives an estimated molecular mass in the range of 2 – 6 million Da, while the DLS analysis yields hydrodynamic radii of 22 – 42 nm (Fig. 5D). The data suggest that *s*NUCB1 binds to and stabilizes a high molecular mass prefibrillar hIAPP species. Analysis of Peak 2 shows a 97–99 kDa molecular mass species with a hydrodynamic radius of 6.2 nm (Fig. 5D), consistent with the value observed for a dimer of *s*NUCB1.

Scanning transmission electron microscopy (STEM) was used to estimate the mass per unit length (M/L) value of the observed prefibrillar species. Dark field images were recorded for the Peak 1 fraction using tobacco mosaic virus (TMV) as an internal standard (Fig. 6). The M/L data were pooled and are presented as histograms. STEM analysis of Peak 1 fraction gave a M/L value ranging from 1 – 7 kDa/Å with the peak of the distribution at 2 kDa/Å (Fig. 6). Goldsbury *et al.* have analyzed hIAPP fibrils using STEM and proposed that 100-nm long protofibrils have a M/L value of approximately 1 kDa/Å and thereby a mass of 1000 kDa[24]. The *s*NUCB1 stabilized prefibrillar species are 40 – 80 nm long and a mean M/L value of 2 kDa/Å assigns an average mass of 1200 kDa to these species. The difference of around 200 kDa is most likely a mass contribution of bound *s*NUCB1. Peak 1 fraction thus consists of protofibril-like species bound to *s*NUCB1 and will be referred to in the following discussion as prefibrillar species. The data strongly argue that Ca^{2+}-free *s*NUCB1 inhibits hIAPP fibril formation by stabilizing prefibrillar species.

As a control, we tested the ability of *s*NUCB1 to bind a monomeric analogue of hIAPP. Pramlintide is a variant of hIAPP that contains 3 Pro substitutions and is known not to aggregate. Isothermal titration calorimetry and SEC experiments showed that pramlintide does not bind Ca^{2+}-free *s*NUCB1 (Fig. S1), suggesting that *s*NUCB1 recognizes a higher order structure of hIAPP, and not hIAPP monomers.

We investigated the stability of the *s*NUCB1-bound prefibrillar species by incubating the Peak 1 fraction at room temperature for 7 days with constant stirring followed by SEC. The same elution profile was observed as had been previously detected for Peak 1. TEM images were recorded on day 1 and on day 7 after elution from the column. The same prefibrillar species were detected for both samples, demonstrating that the *s*NUCB1 stabilized prefibrillar species are stable for at least one week (Fig. S2). These experiments confirm that the *s*NUCB1-bound prefibrillar species are highly stable and do not associate further to form fibrils.

*s*NUCB1 “caps” the ends of prefibrillar intermediates

NUCB1 has no Cys residues, which provides an opportunity to introduce a site-specific reactive sulfhydryl group for labeling with nanogold. A S44C mutant of *s*NUCB1, *s*NUCB1(S44C), was prepared. The mutant was stable in solution and did not aggregate. Control experiments showed that *s*NUCB1(S44C) effectively inhibits hIAPP fibril formation (Fig. S3). We purified nano-Au maleimide labeled *s*NUCB1(S44C) using SEC (Fig. 7A) and observed a labeling efficiency of 1.02 mol/mol, suggesting that each *s*NUCB1(S44C) monomer has a single nano-Au label (Fig. S3). TEM analysis of samples of labeled

*s*NUCB1(S44C) show density for two juxtaposed nano-Au molecules, consistent with the labeling of each monomer subunit in a *s*NUCB1(S44C) dimer (Fig. 7B). We incubated an equimolar amount of nano-Au labeled *s*NUCB1(S44C) with hIAPP and analyzed the resulting mixture after 60 min using TEM. The micrograph shows that the nanogold-labeled mutant inhibits fibril formation by trapping species which appear to be identical to those sequestered by *s*NUCB1. Strikingly, nano-Au density was present only at the ends of the structures and no significant density was observed at any other locations (Fig. 7B). This suggests that *s*NUCB1(S44C) inhibits hIAPP fibril formation by interacting with and capping the ends of the high molecular mass prefibrillar species.

AFM studies were conducted to test the proposed "capping" mechanism. *s*NUCB1 was incubated with equimolar hIAPP and the mixture was analyzed after 60 min using non-contact mode AFM (Fig. 7C). The micrographs show the presence of prefibrillar species with heights varying from 1 – 2 nm and lengths ranging from 40 – 100 nm. Their height is consistent with the protofibrillar species of several aggregating peptides and proteins[25; 26]. Control AFM experiments on hIAPP mature fibrils show that their heights varied from 3 – 5 nm (Fig. S4), which is significantly different from that of the prefibrillar or protofibrillar species observed in Figure 7C. The AFM measurements were repeated using nano-Au labeled *s*NUCB1(S44C). The protein was incubated with hIAPP for 60 min. AFM images show the presence of prefibrillar species with nano-Au density present at the ends as indicated by an increase in height at the ends of the prefibrillar species (Fig. 7D). The AFM data thus strongly suggest that *s*NUCB1 stabilized prefibrillar species are similar to protofibrils of hIAPP, but with *s*NUCB1 capping the ends.

To test whether or not *s*NUCB1 can interact with preformed hIAPP protofibrils, we incubated hIAPP alone for 10 min with constant stirring and then added an equimolar amount of nano-Au labeled *s*NUCB1(S44C). The 10-min time point corresponds to the growth phase of hIAPP aggregation where protofibrils and filaments are formed as monomers are added to the growing nuclei. The reaction mixture was analyzed using AFM. The micrographs reveal hIAPP protofibrils studded with nano-Au labeled *s*NUCB1(S44C) (Fig. 7E). The protofibril in the micrograph is 2 nm in height, consistent with the height reported for typical protofibrils formed from other amyloidogenic proteins[25; 26]. The presence of *s*NUCB1(S44C) along the length of the preformed protofibril shows the interaction of protein with preexisting protofibrils or protofilaments of hIAPP.

Prefibrillar species in complex with sNUCB1 do not seed amyloid fibril formation

We tested the ability of *s*NUCB1 bound prefibrillar species to seed hIAPP fibril formation. Seeding refers to the addition of preformed nuclei into a solution of unaggregated protein. Addition of the seed shortens or bypasses the lag phase. Incubation of hIAPP with seeds generated from sonication of normal hIAPP fibrils shortens the lag phase of the aggregation process and increases the rate of fibril formation (Fig. 8). We then tested the ability of the sNUCB1-stabilized species to seed amyloid formation. In this experiment *s*NUCB1 was incubated with equimolar hIAPP and the reaction mixture was fractionated using SEC. The *s*NUCB1 stabilized prefibrillar species isolated as Peak 1 were then used to "seed" an hIAPP fibrillization reaction. Incubation of hIAPP with increasing amounts of the Peak 1 fraction had no significant affect on the lag phase of the process (Fig. 8). This shows that *s*NUCB1-stabilized prefibrillar species cannot "seed" hIAPP amyloid formation and suggest that they are a "dead-end" entity unable to support further growth.

A second complementary set of seeding studies was preformed using nano-Au labeled hIAPP seeds. Unlabeled hIAPP fibrils were sonicated to generate smaller fragments and labeled with nano-Au under reducing conditions. These labeled fibril fragments were then used to "seed" amyloid formation by unlabeled hIAPP. Figure 8 shows the incorporation of

labeled protofibrils into a growing hIAPP amyloid fibril. Bidirectional growth was observed. The bidirectional growth of nano-Au labeled seeds into amyloid fibrils has been demonstrated for NM fibers[27]. The experiment was repeated using the *s*NUCB1 stabilized hIAPP prefibrillar complex as a seed. The Peak 1 fraction was collected and labeled with nano-Au under reducing conditions. Since *s*NUCB1 contains no Cys residues, only hIAPP is labeled with nano-Au in this experiment (Fig. 8). The nano-Au labeled material was added to unlabeled hIAPP. TEM images of samples withdrawn from the aggregation reaction show that no nano-AU is incorporated into the fibrils and thus confirms that the sNUCB1 stabilized complex does not seed fibril formation (Fig. 8). This result is consistent with the thio-T monitored seeding experiment and confirms that the *s*NUCB1 stabilized prefibrillar species are dead-end products that cannot seed hIAPP aggregation.

We ruled out proteolytic activity of *s*NUCB1 as a mechanism of action using a fluorescence substrate-based protease assay with BODIPY FL-casein as the substrate. Addition of even a 10-fold molar excess of *s*NUCB1 did not result in any notable enhancement in fluorescence intensity (Fig. S5). SDS-PAGE analyses of the samples withdrawn from the reaction mixtures confirm that *s*NUCB1 does not cleave the BODIPY FL-Casein substrate (Fig. S5). Liquid chromatography-mass spectrometry (LC-MS) of mixtures of Ca^{2+}-free *s*NUCB1 and hIAPP provides a third independent test. The mass spectrum shows peaks due to *s*NUCB1 and hIAPP but no apparent lower molecular weight peaks (Fig. S5).

DISCUSSION

The data presented here show that *s*NUCB1 inhibits hIAPP fibril formation in a dose-dependent manner. Importantly, our results show that Ca^{2+}-free *s*NUCB1 can inhibit fibril formation when added during either the nucleation or growth phases of amyloidogenesis. Thus, if aggregation of hIAPP has been initiated, *s*NUCB1 can still prevent the growth of existing amyloidogenic intermediates into fibrils. Intriguingly, *s*NUCB1 also efficiently disaggregates the preformed fibrils. Functionally, molecules with these properties of stage-independent inhibition and disaggregation offer the exciting possibility of being able to clear existing amyloid aggregates, while preventing further sequestration of functional monomers into amyloid deposits.

Our mechanistic studies show that *s*NUCB1 interacts with prefibrillar aggregates of hIAPP to form stable 2 – 6 million Da complexes that can be isolated by SEC. The heterogeneous complexes have hydrodynamic radii ranging from 22 – 42 nm, with a predominant mass density similar to the distribution observed for normal hIAPP protofibrils[24]. The nano-Au labeling studies demonstrate that *s*NUCB1 stabilizes these prefibrillar aggregates by capping their ends. The capped prefibrillar species do not aggregate even when incubated for over a week and are unable to seed the aggregation of hIAPP monomers to form amyloid fibrils, indicating that the capped prefibrillar complex is inert and does not get incorporated into a growing fibril. A similar capping mechanism has been proposed for small molecule inhibitors of amyloid formation, but to the best of our knowledge, *s*NUCB1 is the first protein based inhibitor which has been shown to act by capping protofibrils[28; 29]

The AFM studies show that preformed protofibrils interact with nano-Au labeled *s*NUCB1(S44C). This possibly provides a prototypical snapshot of how *s*NUCB1 may interact with protofibrils and eventually fibrils to facilitate disaggregation. For a self-assembly process like amyloidogenesis, the kinetics of growth can often be dominated by secondary nucleation events resulting from fibril fragmentation[30; 31; 32; 33]. *s*NUCB1 can effectively disaggregate amyloid fibrils and this might be accomplished through interaction with products of hIAPP fibril fragmentation or secondary nuclei. The binding of *s*NUCB1 to

these secondary nuclei would shift the equilibrium of the process in the favor of fibril fragmentation.

The inhibition of hIAPP fibril formation and disaggregation of preformed fibrils by *s*NUCB1 occurs only in the absence of Ca^{2+}. We recently reported that *s*NUCB1 is asymmetric in shape and the dimeric *s*NUCB1 undergoes secondary structure transition from predominantly α-helical to β-sheet as a function of concentration[23]. This structural transition might facilitate the interaction of *s*NUCB1 with pre-fibrillar aggregates of hIAPP, which also possess β-sheet structure. Intriguingly, the C-terminal fragment of NUCB1 has a poly-glutamine (poly-Q) stretch. Poly-Q stretches are unstructured motifs that facilitate protein-protein interaction. In future work, we will characterize an engineered a mutant of *s*NUCB1 that does not bind to Ca^{2+}.

The precise relationship of our findings to the physiological role of NUCB1 is, as of yet, unknown. However, NUCB1 has been reported to be upregulated in the ER-mediated unfolded protein response (UPR). NUCB1 apparently inhibits site-1 protease (S1P)-mediated activating transcription factor 6 (AFT6) cleavage without affecting AFT6 transport and thus prevents UPR activation. ER stress induces NUCB1 secretion from Golgi and increased intracellular NUCB1 expression (29). It is conceivable that NUCB1 controls the UPR by sensing the presence of unfolded proteins in the ER. The observed anti-amyloidogenic activity of *s*NUCB1 is nucleotide independent. However, it is possible that NUCB1 caps these prefibrillar species *in vivo* and assists the chaperone machinery in clearing these complexes while they are still soluble.

METHODS

Thio-T binding assay

Enhancement in thio-T fluorescence was used to monitor the kinetics of hIAPP aggregation in the absence and presence of Ca^{2+}-free *s*NUCB1. All fluorescence measurements were done on a Jobin-Yvon Horiba fluorescence spectrophotometer using an excitation wavelength of 450 nm and an emission wavelength of 485 nm. The emission and excitation slits were both set to 5 nm and a 1.0 cm cuvette was used. Experiments were performed by diluting a HFIP stock solution of hIAPP into 20 mM Tris-HCl, pH 7.5. Each stock solution was filtered through a 0.45 μm pore size GHP Acrodisc syringe filter prior to the experiment. The final reaction mixture contained hIAPP with or without Ca^{2+}-free *s*NUCB1 along with 32 μM thio-T and 2% HFIP in the reaction buffer of 20mM Tris-HCl, pH 7.5. Experiments were conducted at 25 °C with constant stirring. The fluorescence intensity observed for binding of thio-T to Ca^{2+}-free *s*NUCB1 alone was subtracted from each kinetic curve.

Transmission Electron Microscopy (TEM)

Transmission Electron Microscopy (TEM) was performed at the Bioimaging facility at Rockefeller University. Samples were prepared by placing 5 μl of solution onto formvar coated 300 mesh copper grids and counterstained with 2% aqueous uranyl acetate solution. Samples were viewed with a FEI Tecnai12 BioTwinG^2 transmission electron microscope at 80 kV. Digital images were acquired with an AMT XR-60 CCD Digital Camera System and compiled using Adobe Photoshop CS2 and ImageJ.

Atomic Force Microscopy (AFM)

Samples were adsorbed onto freshly cleaved mica from a dilute buffer solution of 20 mM Tris-HCl, pH 7.5 and left to dry. AFM imaging was performed in air once the samples were completely dry. AFM measurements were taken on a Park Systems, XE-100 in True Non

Contact Mode. Rectangular silicon cantilevers were used (Nanosensors, Neuchatel, Switzerland) (NCHR, f = 330kHz, k=42N/m). Non-contact mode images were taken at scan rates between 0.3 and 1 Hz.

Size Exclusion Chromatography

Size exclusion chromatography (SEC) was performed using a Superose6 10 / 30 GL column attached to an AKTA explorer FPLC. 200 μl of a reaction mixture with Ca^{2+}-free sNUCB1 (32 μM) in 20 mM Tris-HCl, pH 7.5 or Ca^{2+}-free sNUCB1 preincubated with equimolar amount of hIAPP in reaction buffer were injected onto a buffer equilibrated column. The chromatogram corresponding to absorbance at 280 nm was plotted as a function of elution volume for each reaction.

Dot Blot Assay

Dot blots were performed by blotting samples onto an activated polyvinylidene fluoride (PVDF) membrane, allowing them to dry and then blocking with 5 % milk solution in TBS (20 mM Tris-HCl, pH 7.5, 150 mM NaCl) at room temperature. The membrane was incubated with a solution of rabbit polyclonal primary antibody against hIAPP (1:2 dilution of prediluted stock) or NUCB1 (1:500 dilution of 1 μg / μl stock) in TBS for 1 h at room temperature followed by three washes with TBS-T (20 mM Tris-HCl, pH 7.5, 150 mM NaCl, 0.05 % Tween-20) for 5 min each. The membranes were then incubated with horseradish peroxidase conjugated anti-rabbit secondary antibody (1:8000 dilution of the stock) in TBS for 30 min at room temperature followed by two washes with TBS-T for 5 min each and a subsequent wash with TBS for 5 min. The blots were developed using the supersignal west femto maximum sensitivity substrate (Thermo Scientific).

Scanning Transmission Electron Microscopy (STEM) and mass per unit length measurements

Dark-field micrographs of unstained freeze-dried specimens together with TMV particles as a mass standard were prepared according to the standard “wet film” method of the Brookhaven STEM facility. This involved freeze-drying the sample with TMV on titanium grids supporting a 2 - to 3 - nm carbon film. Grids were scanned at −150 °C on a custom-built STEM at 40 kV with a probe focused to 0.25 nm with a dwell time of 30 μs / pixel. Digital dark-field micrographs of freeze-dried specimens were recorded with 512 × 512 pixels at raster steps of 1.0 or 2.0 nm per pixel and an average radiation dose of 1 × 102 to 5 × 102 electron / nm2. The images were analyzed using the PCMass30 software (Brookhaven STEM resource). The resulting data were normalized to the known mass per unit length of TMV (131.4 kDa / nm).

Light Scattering

Light scattering data was collected using a Superose6 10/30 GL SEC column (GE Healthcare, Piscataway, NJ), connected to High Performance Liquid Chromatography System (HPLC), Agilent 1200, (Agilent Technologies, Wilmington, DE) equipped with an autosampler. The elution from SEC was monitored by a photodiode array (PDA) UV / VIS detector (Agilent Technologies, Wilmington, DE), differential refractometer (OPT-Lab rEx Wyatt Corp., Santa Barbara, CA), static and dynamic, multiangle laser light scattering (LS) detector (HELEOS II with QELS capability, Wyatt Corp., Santa Barbara, CA). The SEC-UV / LS / RI system was pre-equilibrated in buffer (20 mM Tris-HCl, pH 7.5) and 200 μl of reaction mixture containing either Ca^{2+}-free sNUCB1 alone or incubated with an equimolar amount of hIAPP were injected onto the column. Chemstation software (Agilent Technologies, Wilmington, DE) controlled the HPLC operation and data collection from the multi-wavelength UV / VIS detector, while the ASTRA software (Wyatt Corp., Santa

Barbara, CA) collected data from the refractive index (RI) detector, the light scattering detectors, and recorded the UV trace at 280 nm sent from the PDA detector. Molecular masses were determined across the entire elution profile for each observed peak in intervals of 1 sec from static LS measurement using ASTRA software as previously described[34]. Dynamic light scattering (DLS) measurements were made “on line” at an angle of 100° with a 2 sec collection time across the elution peaks. Time resolved scatter intensity fluctuations were analyzed using ASTRA Software (Wyatt Corp., Santa Barbara, CA) which implements the cumulants method[35] to determine the intensity correlation function.

Supplementary Material

Refer to Web version on PubMed Central for supplementary material.

Acknowledgments

This work was supported by NIH-GMO78114 (to D.P.R) and by the Eleanor Schwartz Charitable Trust and the Bridges to Better Medicine Fund (to T.P.S). We thank Dr. W Vallen Graham for helpful discussions. We also thank Ms. Trisha Barua, Dr. Fanling Meng and Ms. Ping Cao of Stony Brook University for preparing hIAPP. We gratefully acknowledge the assistance of Dr. Ewa Folta-Stogniew of the Keck Foundation Biotechnology Resource Laboratory, Yale University School of Medicine, Dr. Joseph Wall, Brookhaven National Laboratory, Dr. Hiro Uryu, Rockefeller University Electron Microscopy Resource Center, and Dr. Cynthia Buenviaje-Coggins and Ying Xiong of Park AFM Systems.

Abbreviations

AFM	Atomic Force Microscopy
DLS	Dynamic Light Scattering
DM	Diabetes Mellitus
hIAPP	human Islet Amyloid Polypeptide
MALS	Multi-angle Light Scattering
NUCB1	Nucleobindin 1
***s*NUCB1**	Soluble NUCB1
SEC	size exclusion chromatography
STEM	Scanning Transmission Electron Microscopy
TEM	Transmission Electron Microscopy
thio-T	thioflavin-T
UPR	Unfolded Protein Response

References

1. Chiti F, Dobson CM. Protein misfolding, functional amyloid, and human disease. Annu Rev Biochem. 2006; 75:333–366. [PubMed: 16756495]
2. Caughey B, Lansbury PT. Protofibrils, pores, fibrils, and neurodegeneration: separating the responsible protein aggregates from the innocent bystanders. Annu Rev Neurosci. 2003; 26:267–298. [PubMed: 12704221]
3. Selkoe DJ. Cell biology of protein misfolding: the examples of Alzheimer's and Parkinson's diseases. Nat Cell Biol. 2004; 6:1054–1061. [PubMed: 15516999]
4. Halfmann R, Alberti S, Lindquist S. Prions, protein homeostasis, and phenotypic diversity. Trends Cell Biol. 2010; 20:125–133. [PubMed: 20071174]

5. Chen S, Ferrone FA, Wetzel R. Huntington's disease age-of-onset linked to polyglutamine aggregation nucleation. Proc Natl Acad Sci U S A. 2002; 99:11884–11889. [PubMed: 12186976]
6. Antzutkin ON, Leapman RD, Balbach JJ, Tycko R. Supramolecular structural constraints on Alzheimer's beta-amyloid fibrils from electron microscopy and solid-state nuclear magnetic resonance. Biochemistry. 2002; 41:15436–15450. [PubMed: 12484785]
7. Luca S, Yau WM, Leapman R, Tycko R. Peptide conformation and supramolecular organization in amylin fibrils: constraints from solid-state NMR. Biochemistry. 2007; 46:13505–13522. [PubMed: 17979302]
8. Kayed R, Head E, Thompson JL, McIntire TM, Milton SC, Cotman CW, Glabe CG. Common structure of soluble amyloid oligomers implies common mechanism of pathogenesis. Science. 2003; 300:486–489. [PubMed: 12702875]
9. Lorenzo A, Razzaboni B, Weir GC, Yankner BA. Pancreatic islet cell toxicity of amylin associated with type-2 diabetes mellitus. Nature. 1994; 368:756–760. [PubMed: 8152488]
10. Enoki S, Mitsukawa T, Takemura J, Nakazato M, Aburaya J, Toshimori H, Matsukara S. Plasma islet amyloid polypeptide levels in obesity, impaired glucose tolerance and non-insulin-dependent diabetes mellitus. Diabetes Res Clin Pract. 1992; 15:97–102. [PubMed: 1541241]
11. Kahn SE, Andrikopoulos S, Verchere CB. Islet amyloid: a long-recognized but underappreciated pathological feature of type 2 diabetes. Diabetes. 1999; 48:241–253. [PubMed: 10334297]
12. Wookey PJ, Lutz TA, Andrikopoulos S. Amylin in the periphery II: An updated mini-review. Scientific World Journal. 2006; 6:1642–1655. [PubMed: 17173182]
13. Clark A, Nilsson MR. Islet amyloid: a complication of islet dysfunction or an aetiological factor in Type 2 diabetes? Diabetologia. 2004; 47:157–169. [PubMed: 14722650]
14. Yan LM, Tatarek-Nossol M, Velkova A, Kazantzis A, Kapurniotu A. Design of a mimic of nonamyloidogenic and bioactive human islet amyloid polypeptide (IAPP) as nanomolar affinity inhibitor of IAPP cytotoxic fibrillogenesis. Proc Natl Acad Sci U S A. 2006; 103:2046–2051. [PubMed: 16467158]
15. Moriarty DF, Raleigh DP. Effects of sequential proline substitutions on amyloid formation by human amylin20–29. Biochemistry. 1999; 38:1811–1818. [PubMed: 10026261]
16. Mishra R, Bulic B, Sellin D, Jha S, Waldmann H, Winter R. Small-molecule inhibitors of islet amyloid polypeptide fibril formation. Angew Chem Int Ed Engl. 2008; 47:4679–4682. [PubMed: 18470855]
17. Meng F, Abedini A, Plesner A, Middleton CT, Potter KJ, Zanni MT, Verchere CB, Raleigh DP. The sulfated triphenyl methane derivative acid fuchsin is a potent inhibitor of amyloid formation by human islet amyloid polypeptide and protects against the toxic effects of amyloid formation. J Mol Biol. 2010; 400:555–566. [PubMed: 20452363]
18. Meng F, Abedini A, Plesner A, Verchere CB, Raleigh DP. The flavanol (−)-epigallocatechin 3-gallate inhibits amyloid formation by islet amyloid polypeptide, disaggregates amyloid fibrils, and protects cultured cells against IAPP-induced toxicity. Biochemistry. 2010; 49:8127–8133. [PubMed: 20707388]
19. Saraogi I, Hebda JA, Becerril J, Estroff LA, Miranker AD, Hamilton AD. Synthetic alpha-helix mimetics as agonists and antagonists of islet amyloid polypeptide aggregation. Angew Chem Int Ed Engl. 2010; 49:736–739. [PubMed: 20029853]
20. Gazit E. Mechanisms of amyloid fibril self-assembly and inhibition. Model short peptides as a key research tool. FEBS J. 2005; 272:5971–5978. [PubMed: 16302962]
21. Kawano J, Kotani T, Ogata Y, Ohtaki S, Takechi S, Nakayama T, Sawaguchi A, Nagaike R, Oinuma T, Suganuma T. CALNUC (nucleobindin) is localized in the Golgi apparatus in insect cells. Eur J Cell Biol. 2000; 79:208–217. [PubMed: 10777113]
22. Lin P, Fischer T, Lavoie C, Huang H, Farquhar MG. Calnuc plays a role in dynamic distribution of Galphai but not Gbeta subunits and modulates ACTH secretion in AtT-20 neuroendocrine secretory cells. Mol Neurodegener. 2009; 4:15. [PubMed: 19320978]
23. Kapoor N, Gupta R, Menon ST, Folta-Stogniew E, Raleigh DP, Sakmar TP. Nucleobindin 1 is a calcium-regulated guanine nucleotide dissociation inhibitor of G{alpha}i1. J Biol Chem. 2010; 285:31647–31660. [PubMed: 20679342]

24. Goldsbury C, Goldie K, Pellaud J, Seelig J, Frey P, Muller SA, Kistler J, Cooper GJ, Aebi U. Amyloid fibril formation from full-length and fragments of amylin. J Struct Biol. 2000; 130:352–362. [PubMed: 10940238]
25. Hoos MD, Ahmed M, Smith SO, Van Nostrand WE. Myelin basic protein binds to and inhibits the fibrillar assembly of Abeta42 in vitro. Biochemistry. 2009; 48:4720–4727. [PubMed: 19385666]
26. Srinivasan R, Jones EM, Liu K, Ghiso J, Marchant RE, Zagorski MG. pH-dependent amyloid and protofibril formation by the ABri peptide of familial British dementia. J Mol Biol. 2003; 333:1003–1023. [PubMed: 14583196]
27. Scheibel T, Kowal AS, Bloom JD, Lindquist SL. Bidirectional amyloid fiber growth for a yeast prion determinant. Curr Biol. 2001; 11:366–369. [PubMed: 11267875]
28. Sievers SA, Karanicolas J, Chang HW, Zhao A, Jiang L, Zirafi O, Stevens JT, Munch J, Baker D, Eisenberg D. Structure-based design of non-natural amino-acid inhibitors of amyloid fibril formation. Nature. 2011
29. Zheng J, Liu C, Sawaya MR, Vadla B, Khan S, Woods RJ, Eisenberg D, Goux WJ, Nowick JS. Macrocyclic beta-sheet peptides that inhibit the aggregation of a tau-protein-derived hexapeptide. J Am Chem Soc. 2011; 133:3144–3157. [PubMed: 21319744]
30. Xue WF, Homans SW, Radford SE. Systematic analysis of nucleation-dependent polymerization reveals new insights into the mechanism of amyloid self-assembly. Proc Natl Acad Sci U S A. 2008; 105:8926–8931. [PubMed: 18579777]
31. Collins SR, Douglass A, Vale RD, Weissman JS. Mechanism of prion propagation: amyloid growth occurs by monomer addition. PLoS Biol. 2004; 2:e321. [PubMed: 15383837]
32. Knowles TP, Waudby CA, Devlin GL, Cohen SI, Aguzzi A, Vendruscolo M, Terentjev EM, Welland ME, Dobson CM. An analytical solution to the kinetics of breakable filament assembly. Science. 2009; 326:1533–1537. [PubMed: 20007899]
33. Bishop MF, Ferrone FA. Kinetics of nucleation-controlled polymerization. A perturbation treatment for use with a secondary pathway. Biophys J. 1984; 46:631–644. [PubMed: 6498276]
34. Folta-Stogniew E, Williams K. Determination of molecular masses of proteins in solution: Implementation of an HPLC size exclusion chromatography and laser light scattering service in a core laboratory. J Biomol Tech. 1999; 10:51–63. [PubMed: 19499008]
35. Koppel DE. Analysis of Macromolecular Polydispersity in Intensity Correlation Spectroscopy - Method of Cumulants. Journal of Chemical Physics. 1972; 57 4814-&.

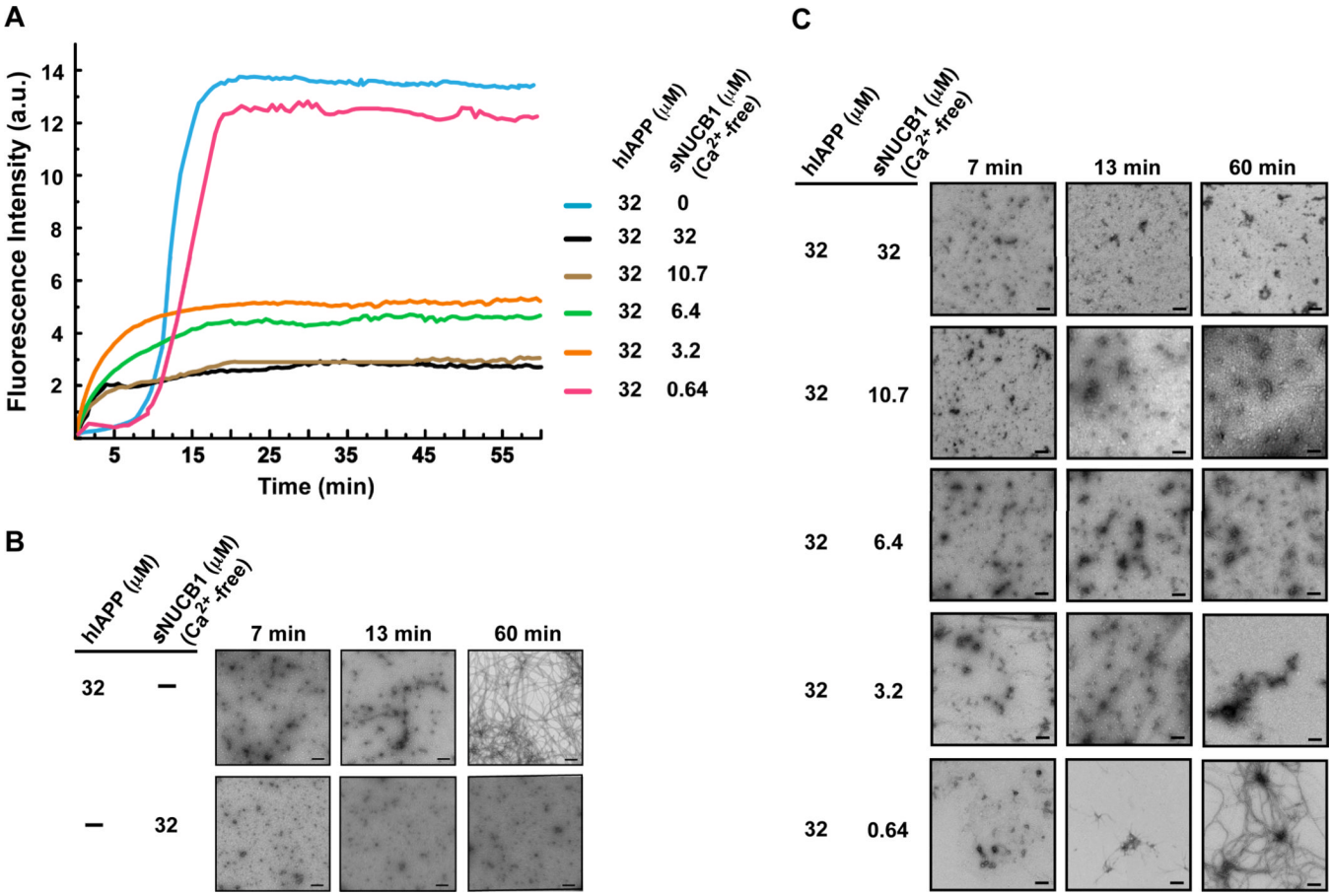

Figure 1. Ca^{2+}-free *s*NUCB1 inhibits hIAPP fibril formation in a dose-dependent manner

(A) The kinetics of hIAPP aggregation was monitored using fluorescence detected thio-T binding assays. Aggregation of hIAPP alone shows an initial nucleation phase, which then extends into a rapid growth phase. The aggregation continues and reaches a plateau indicating the formation of amyloid fibrils. Incubation of hIAPP with stoichiometric or sub-stoichiometric concentrations of Ca^{2+}-free *s*NUCB1 shows significant inhibition of fibril formation. Each reaction was also monitored using TEM. As a control **(B)** hIAPP and Ca^{2+}-free *s*NUCB1 were incubated alone and samples were withdrawn at 7 min, 13 min and 60 min. hIAPP alone aggregates rapidly to form fibrils within 60 min whereas Ca^{2+}-free *s*NUCB1 alone does not form higher order aggregates. **(C)** TEM analysis of the reaction mixtures presented in Panel A confirms that Ca^{2+}-free *s*NUCB1 inhibits hIAPP amyloid formation. Scale bars represent 200 nm.

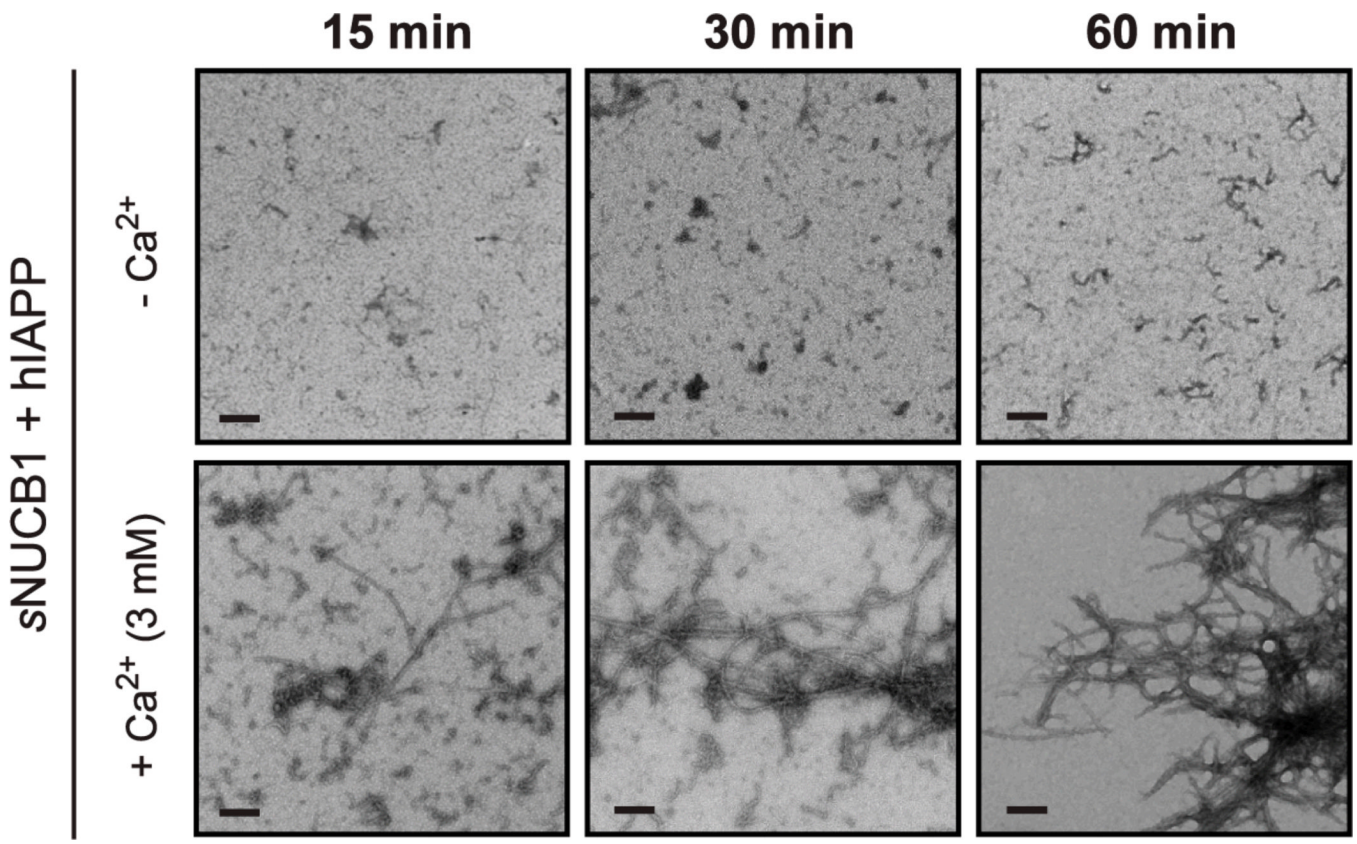

Figure 2. The anti-amyloidogenic activity of *s*NUCB1 is Ca^{2+}-dependent

The aggregation of hIAPP was monitored in the presence of equimolar *s*NUCB1. In the absence of Ca^{2+}, *s*NUCB1 effectively inhibit hIAPP fibril formation when added at T = 0. When excess Ca^{2+} (3 mM) is present in the reaction mixture, *s*NUCB1 does not inhibit hIAPP fibril formation.

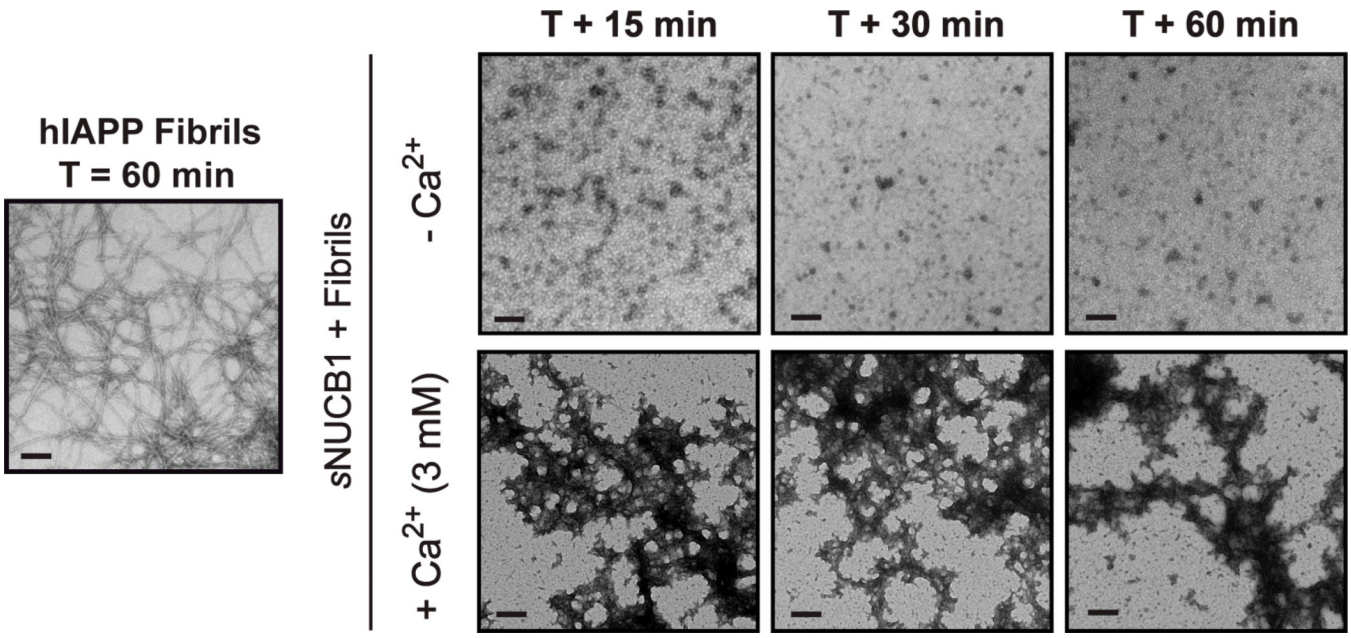

Figure 3. Ca^{2+} free *s*NUCB1 disaggregates of hIAPP fibrils

In the absence of Ca^{2+}, *s*NUCB1 effectively disaggregates amyloid fibrils within 15 min of the addition. Disaggregation persists even in samples withdrawn at 30 min and 60 min. In the presence of excess Ca^{2+} (3 mM), *s*NUCB1 does not disaggregate hIAPP fibrils. TEM analysis shows the presence of fibrillar aggregates at all monitored time points. Scale bars represent 200 nm.

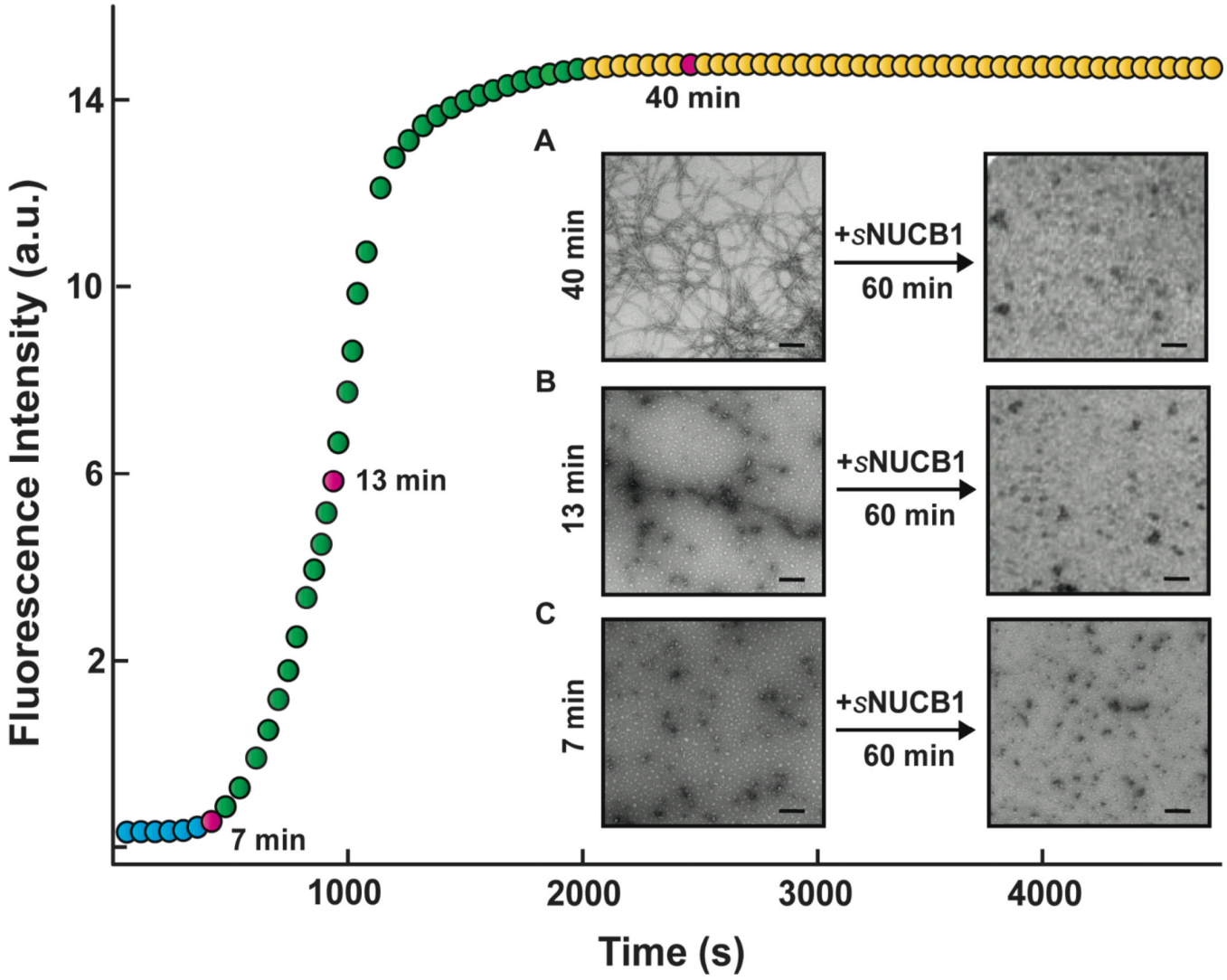

Figure 4. Ca^{2+}-free *s*NUCB1 inhibits hIAPP amyloidogenesis in a state-independent manner

hIAPP (32 μM) aggregation was monitored using thio-T (32 μM). The lag phase is shown in blue, the growth phase in green and the stationary phase in yellow. Aggregation was allowed to proceed to (A) the nucleation phase at 7 min, (B) the mid-point of growth phase at 15 min and (C) the initiation of stationary phase at 40 min. At the indicated time, samples were removed and an equimolar amount (32 μM) of Ca^{2+}-free *s*NUCB1 was added. The pink circles indicate the time points at which *s*NUCB1 was added. TEM images were collected immediately before addition of *s*NUCB1 and 60 min after addition of *s*NUCB1. The micrographs corresponding to samples withdrawn at 60 min after addition show that Ca^{2+}-free *s*NUCB1 both effectively inhibits the progression of seeds into mature fibrils and disaggregates mature fibrils. Scale bars represent 200 nm.

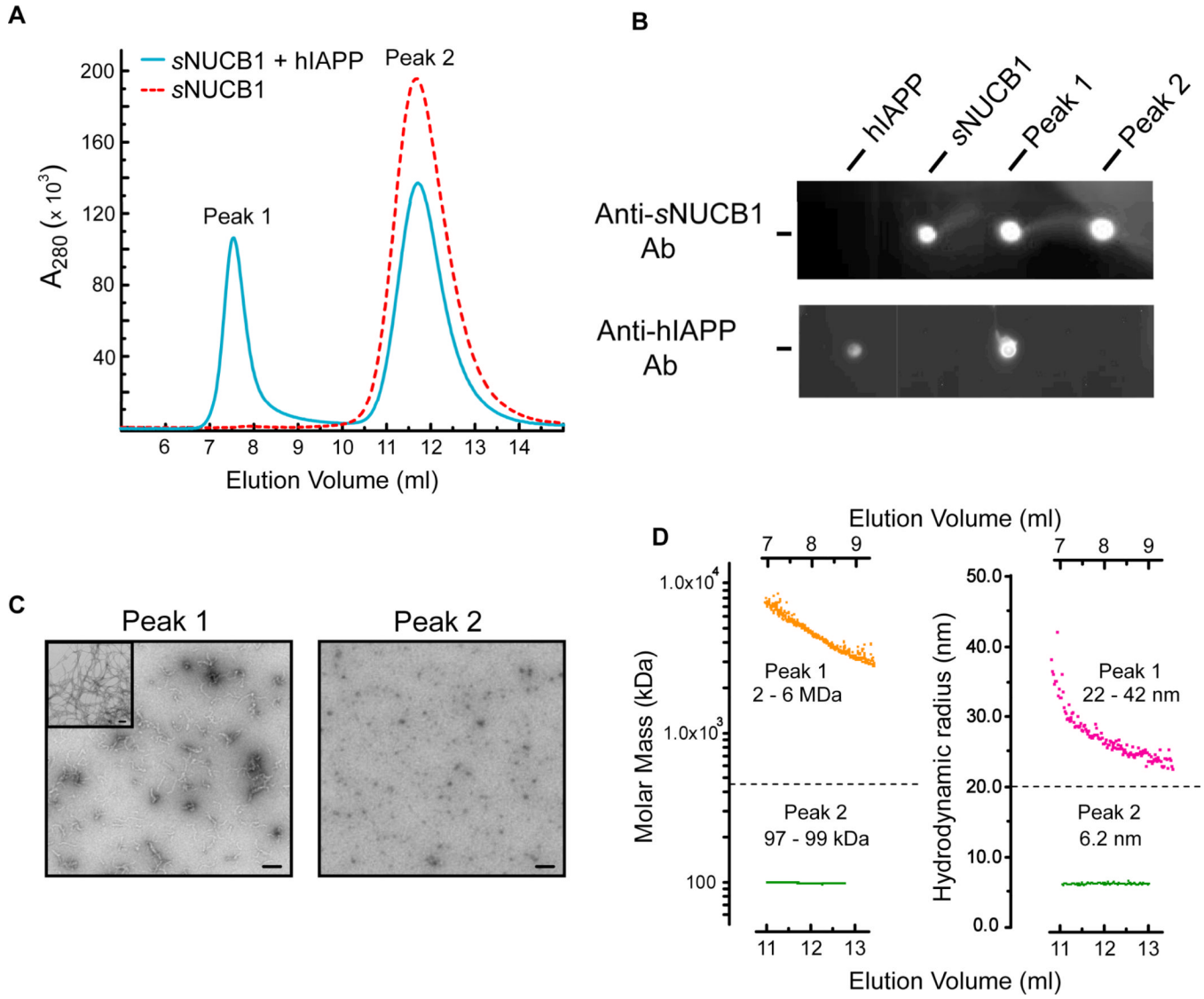

Figure 5. Biophysical characterization of Ca^{2+}-free *s*NUCB1 stabilized hIAPP prefibrillar species

(A) SEC was used to analyze the products of the 1:1 mixture of hIAPP and Ca^{2+}-free *s*NUCB1. Ca^{2+}-free *s*NUCB1 alone elutes at 12 ml (red dotted curve) while the sample from a 1:1 reaction mixture removed after 60 min gives an additional peak, Peak1, eluting at 7.8 ml. **(B)** Dot-blot assay shows that *s*NUCB1 is present in both peaks, hIAPP is only present in the Peak 1 fraction. **(C)** TEM analysis of the Peak1 fraction shows the presence of oligomeric and prefibrillar species whereas no higher order aggregates were observed in the Peak 2 fraction. Insert: TEM image of fibrils alone. **(D)** MALS analysis (left) across Peak1 estimates the molecular mass in the range of 2 – 6 million Da and DLS (right) predicts hydrodynamic radii in the range of 22 – 42 nm. MALS and DLS analysis of Peak2 predicts a molecular mass and hydrodynamic radii characteristic for a dimer of *s*NUCB1.

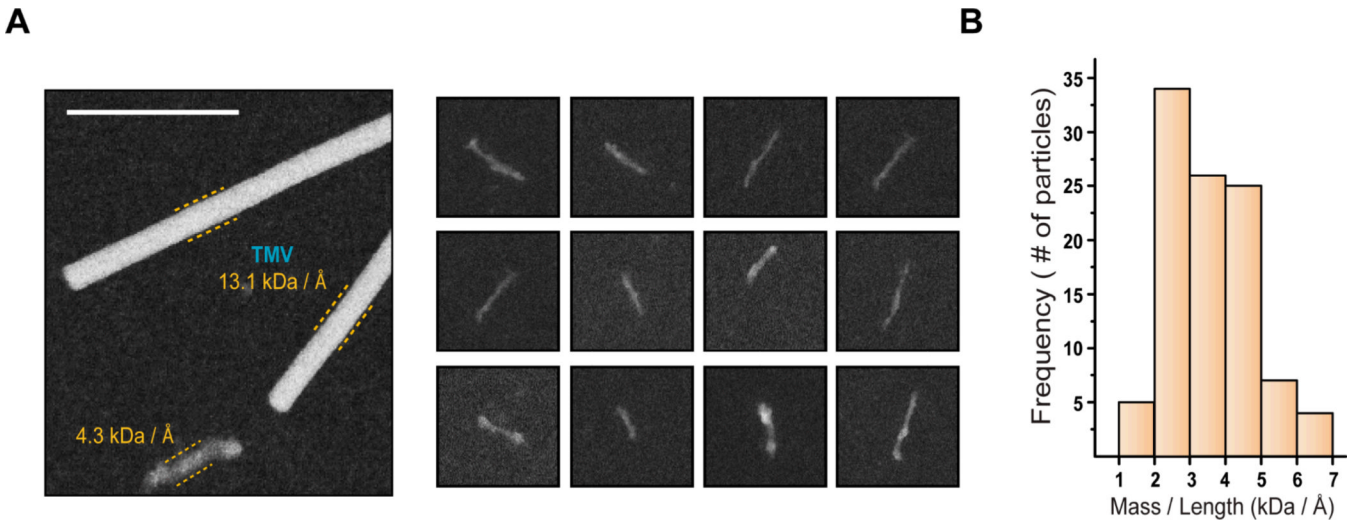

Figure 6. *s*NUCB1 stabilizes hIAPP protofibrillar species

STEM was used to determine the mass / unit length (M / L) distribution of prefibrillar species in the Peak1 fraction. **(A)** The image shows a typical dark-field cryo-STEM image of the Peak1 fraction. The adjacent panel shows images representing prefibrillar species observed in STEM. The scale bar or width of each box represents 100 nm. **(B)** Quantitative analysis shows the presence of prefibrillar species with M / L ranging from 1 – 7 kDa / Å with the predominant species ranging from 2 – 5 kDa / Å.

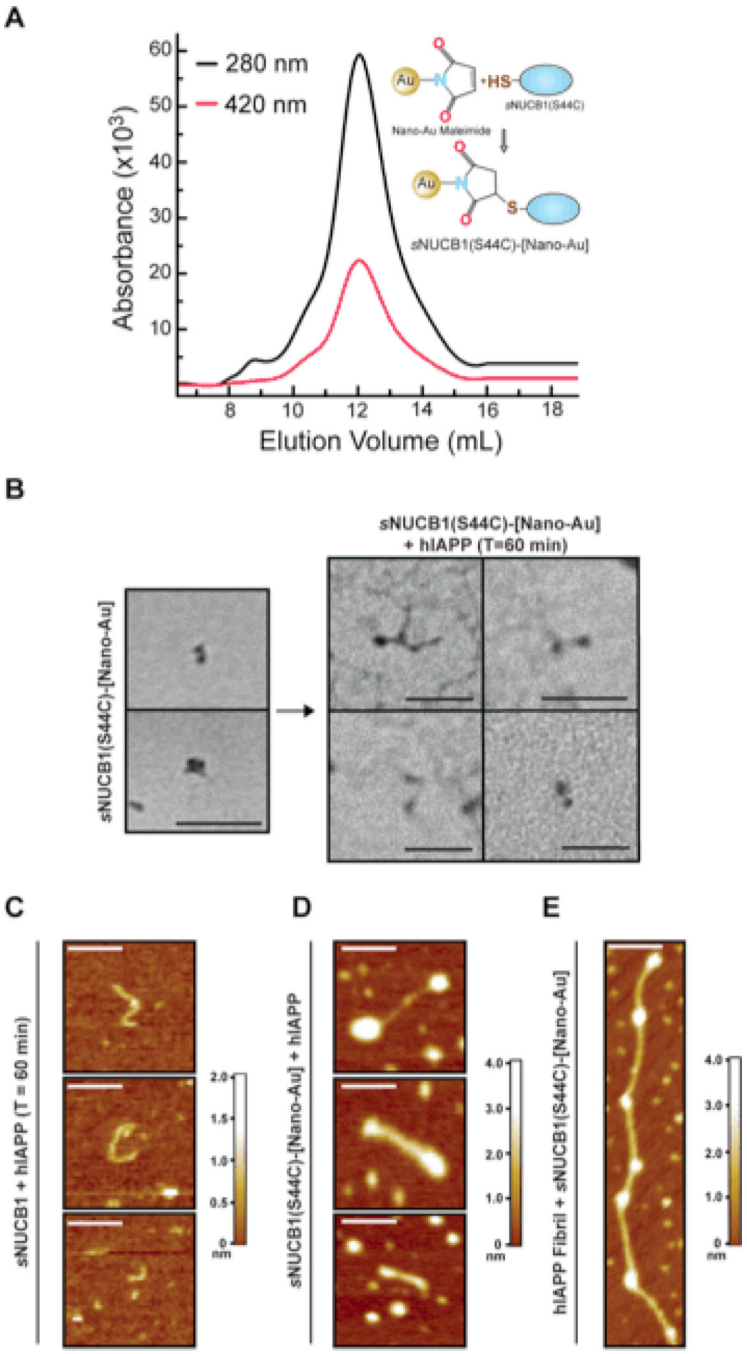

Figure 7. Nano-Au labeled *s*NUCB1(S44C) "caps" hIAPP prefibrillar species

(A) Nano-Au labeled *s*NUCB1(S44C) was purified via SEC. The chromatogram shows the co-elution of the 280-nm protein peak (black) and the 420-nm nano-Au peak (red). The inset shows a schematic of the conjugation reaction that covalently links the nano-Au to a Cys residue. **(B)** TEM analysis of the labeled sample shows the presence of two typical nano-Au densities corresponding to a dimer of a labeled *s*NUCB1(S44C). Nano-Au labeled *s*NUCB1(S44C) was incubated with equimolar hIAPP for 60 min after which samples were withdrawn. TEM analysis shows the presence of high molecular mass prefibrillar species with labeled ends. The scale bar represents 100 nm. AFM in non-contact mode was used to

corroborate the TEM studies. **(C)** The micrographs reveal *s*NUCB1 stabilized hIAPP prefibrillar species with the height of prefibrillar species varying from 1.0 to 2.0 nm. The inhibition reaction was repeated using purified *s*NUCB1(S44C)-[Nano-Au]. **(D)** AFM images confirm that *s*NUCB1(S44C)-[Nano-Au] caps the ends of prefibrillar species of hIAPP. The presence of Nano-Au clusters was confirmed by increase in height of the ends of these prefibrillar species. **(E)** AFM micrographs show hIAPP protofibrils studded with *s*NUCB1(S44C)-[Nano-Au]. The image illustrates the interaction of *s*NUCB1(S44C) with preformed protofibrils of hIAPP. The scale bar in each AFM image represents 100 nm. The color contour scale on the right of each AFM panel represents the height of each sample in nm. AFM images of mature fibrils are included in the supporting information.

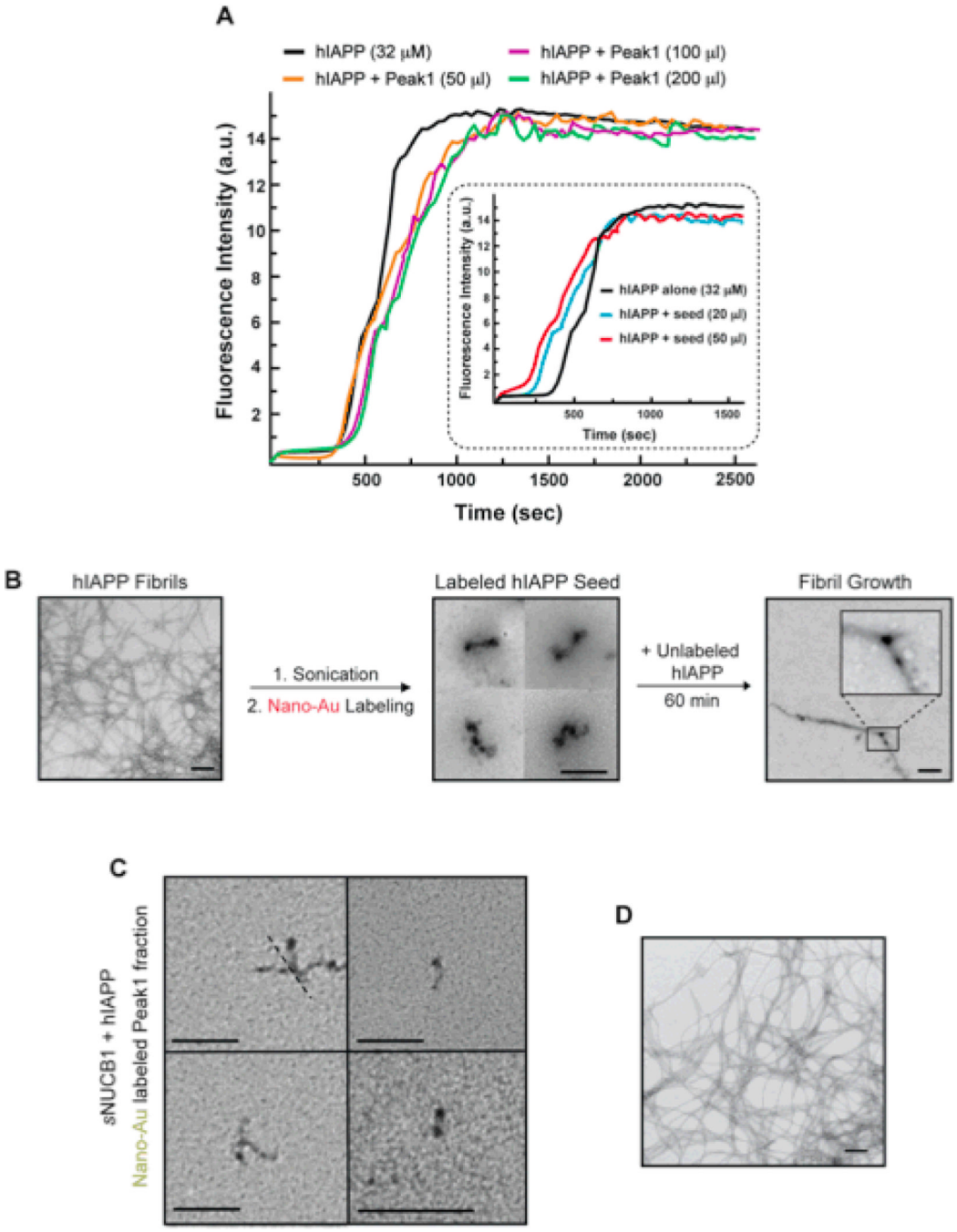

Figure 8. Ca^{2+}-free *s*NUCB1 stabilized hIAPP prefibrillar species are not incorporated into growing fibrils

(A) Aggregation kinetics of hIAPP alone (black) or in the presence of 50 μl (orange), 100 μl (purple) or 200 μl (green) of the Peak 1 fraction monitored using thio-T binding assays. No noticeable shortening of the lag phase was observed. The insert shows a seeding reaction with pure preformed hIAPP amyloid fibers. A significant shortening of the lag phase was observed when 20 μl (blue) or 50 μl (red) pure hIAPP seed was added. To visualize seeding nano-gold labeling was used. **(B)** Nano-gold labeled hIAPP seeds are incorporated into hIAPP fibrils. Pre-formed hIAPP fibrils were sonicated to generate oligomers and protofibrils, labeled with nano-Au and used to seed hIAPP fibrillization. TEM analysis

shows incorporation of the nano-Au labeled aggregate. **(C)** Nano-gold labeled sNUCB1 stabilized labeled prefibrillar species are not incorporated into hIAPP fibrils. The material from Peak1 was labeled with nano-Au and analyzed using TEM. **(D)** The nano-Au labeled prefibrillar species were then incubated with hIAPP and sample was withdrawn at 60 min and analyzed by TEM. The mature hIAPP fibrils do not incorporation the nano-Au labeled, sNUCBI stabilized, prefibrillar species. The scale bars represent 200 nm.